Rare Metal Materials and Engineering
Volume 53, Issue 4, April 2024
Available online at www.rmme.ac.cn

Science Press

Cite this article as: Miao Liguo, Xing Fei, Chai Yuanxin, et al. Prediction Method of Laser-Deposited Melt Pool Width Based on Edge Iterative Model[J]. Rare Metal Materials and Engineering, 2024, 53(04): 978-987. DOI: 10.12442/j.issn.1002-185X.20230356.

ARTICLE

Prediction Method of Laser-Deposited Melt Pool Width Based on Edge Iterative Model

Miao Liguo[1], **Xing Fei**[1,2], **Chai Yuanxin**[1], **Yan Chengxin**[1], **Liu Weijun**[1]

[1] *School of Mechanical Engineering, Shenyang University of Technology, Shenyang 110870, China;* [2] *Nanjing Zhongke Raycham Laser Technology Co., Ltd, Nanjing 210038, China*

Abstract: According to the spatial distribution pattern of melt pool size features, a prediction method of melt pool width based on edge iterative model was proposed. In order to obtain accurate melt pool width, mathematical morphological method was used to denoise the melt pool image and coarse segmentation was conducted on the melt pool image by manual thresholding method. The Canny algorithm was then employed to extract the melt pool edge. Finally, the edge iterative model was used for edge iteration and the melt pool width after fine segmentation was obtained. Comparison experiment results show that this algorithm has good accuracy and robustness, and it is simple and efficient.

Key words: laser metal deposition manufacturing; melt pool; edge iterative model; feature extraction

Laser-directed energy deposition (LDED) is a unique manufacture technique, which uses high-energy laser beam to form melt pool in the deposition area. The laser beam moves at high speed, and the to-be-deposited material is directly fed into the high-temperature melt zone in the powder form and deposited layer by layer after melting. LDED technique has the advantages of high material utilization, fast part forming, and no mold fixtures, which is suitable for the manufacture of complex parts and the repair and remanufacture of valuable parts[1–4]. Melt pool is the smallest forming unit in LDED process. Slight variations in process parameters and deposition environment can cause large fluctuations in the melt pool size, affecting the deposition quality. Therefore, online inspection and closed-loop control of the laser melt pool are essential[5].

Laser processing exhibits high-energy characteristics, and its non-contact visual detection[6–8] is the mainstream detection method in recent years. The key characteristics of melt pool include width, height, depth, area, and temperature, which are usually used for monitoring. Algorithm can also be used to predict the key characteristics of melt pool. Su et al[9] designed an infrared detection system to detect the melt pool edge and then obtained a vector perpendicular to the direction of scanning speed. The maximum value between the abovementioned vector and the melt pool edge is taken as the melt pool width. Zheng et al[10] predicted the melt pool width by extracting the pool boundary from the image, and the prediction error is less than 5%. Sun et al[11] predicted the melt pool width and length by ellipse fitting with prediction accuracy of 95% and 90%, respectively. Le et al[12] calculated the melt pool length and width by counting the pixel points on the horizontal and vertical axes, respectively. Huang et al[13] developed a gas metal arc welding-based binocular vision system to obtain the melt pool width by minimizing the external rectangles. Similar approach is reported in Ref. [14]. The melt pool depth can also be predicted based on the melt pool width data. For example, Jeon et al[15] proposed an online melt pool depth prediction method to predict the melt pool depth during multi-layer multi-pass deposition process. Goossens et al[16] proposed a physically resolved model to calculate the depth-to-width ratio of melt pool based on the process parameters and material properties. Other detection methods of melt pool features have also been investigated. Liu et al[17] developed a real-time online prediction system to estimate the layer height based on the DaNN network within

---

Received date: June 06, 2023

Foundation item: National Key Research and Development Program of China (2022YFB4602200); National Science and Technology Major Project (2019-VII-0004-0144)

Corresponding author: Liu Weijun, Ph. D., Professor, School of Mechanical Engineering, Shenyang University of Technology, Shenyang 110870, P. R. China, E-mail: wjliu@sut.edu.cn

Copyright © 2024, Northwest Institute for Nonferrous Metal Research. Published by Science Press. All rights reserved.

0.018 s. Zhu et al[18] applied deep learning method onto 3D additive manufacture (AM) modeling and accurately predicted the temperature and melt pool dynamics in the AM process of metal materials. Zheng et al[19] adjusted the laser power and scanning speed to achieve the designed cooling rate and size of melt pool. Colodron et al[20] presented a field-programmable gate array-based image processing system with test frame rate of 110 frame/s. Ding et al[21] designed an inspection system to detect powder and melt pool size, but the specific inspection method of melt pool width was not mentioned.

With the development of physical model for LDED process and the improvement in computing capability of hardware, the prediction methods of melt pool characteristics based on simulation data and machine learning are increasingly valued[22–24]. However, a significant gap in prediction accuracy exists among different methods, not to mention the gap between detection accuracy of machine vision and prediction accuracy. Currently, the detection method of online visualized melt pool is the preferred solution for melt pool feature detection. Song et al[25] reported that the melt pool width can better reflect the characteristics of melt pool, compared with other melt pool features. Although the abovementioned edge detection algorithms can detect the melt pool width, serious interference restricts their industrial applications. As shown in Fig. 1, there is noise caused by arc light and powder splash in LDED process. Therefore, the accuracy of melt pool feature extraction can be greatly influenced[26–27]. The melt pool feature extraction methods should be further ameliorated and have strong anti-interference capability.

In this research, a melt pool width extraction algorithm based on edge iterative model coupled with morphology characteristics of melt pool region and processing efficiency of image algorithms was proposed. This algorithm provided practical guidance for the development of stable melt pool edge extraction algorithm with high accuracy and high robustness.

1 Experiment

Fig. 2 shows the experiment system used in this research. The system consisted of AM and image acquisition units. AM unit was mainly composed of Siemens CNC (420D), IPG laser, and deposition head with circular powder feeding mode. The maximum laser power was 2000 W. The light path in the deposition head was controlled by a mounted beam splitter with the angle of 45° for the propagation along both forward and reverse light paths. The forward light path passed the laser with wavelength of 1070±10 nm, and the reverse light path passed the visible light with wavelength of 390 – 780 nm. During the forward propagation, a focusing mirror with focal length of 250 mm focused the beam with diameter of 15.5 mm into spot with diameter of approximately 1.2 mm on the substrate surface. The high temperature laser beam melted the powder to form melt pool, producing reflected light which was reflected to CMOS camera through spectroscope. The CMOS camera was coaxially mounted for high equipment integration and no image distortion. The front end of CMOS camera was equipped with a band-pass filter (540±10 nm) and a neutral density filter (5%). The band-pass filter can improve the image clarity and reduce ambient light interference. The neutral density filter can prevent the incident light range from exceeding the dynamic acquisition range of the camera (73 dB).

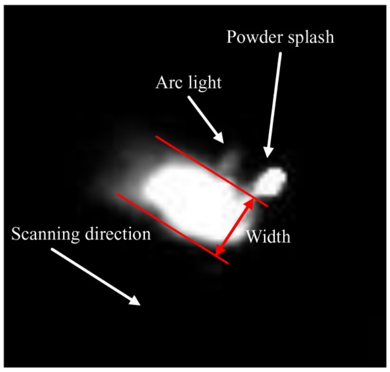

Fig.1 Representative image of melt pool captured by coaxial camera

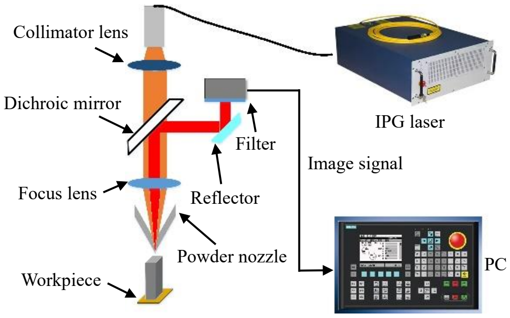

Fig.2 Schematic diagram of coaxial monitoring system

During the experiment, the melt pool was a relatively small part of the whole image, and the image was cropped to improve the image processing efficiency. The raw image resolution was 1024×768, and the resolution of cropped image was 200×192. Fe101 alloy powder was used in the experiment, and its powder particle size ranged from 20 μm to 53 μm. The composition of Fe101 alloy powder is shown in Table 1. The substrate material was 316L alloy, and the diameter of powder spot on the substrate surface was about 1.17 mm, which was located below the laser focus.

2 Principle, Results, and Analysis

The melt pool width extraction process is shown in Fig.3.

2.1 Image preprocessing

Fig. 4 shows the pre-processing results of melt pool image. Fig. 4a shows the raw image of melt pool acquired by the hardware. The laser scanning direction and the melt pool

Table 1 Composition of Fe101 alloy powder (wt%)

C	Mn	Si	Ni	Mo	Cr	N	P	Fe
0.03	0.35	7.86	0.77	14.55	0.12	0.045	0.42	Bal.

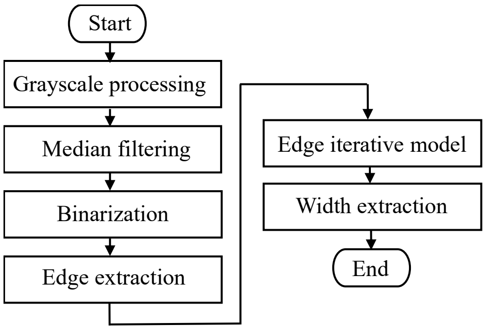

Fig.3 Schematic diagram of melt pool width extraction process

width are marked in Fig.4a. Initially, the raw image is converted to grayscale image and subject to median filtering to enhance computational efficiency and to minimize random noise during data transfer. Subsequently, the image undergoes thresholding for segmentation, which is determined by depositing a single melt and extracting its width data for comparison with the binary image width data under various thresholds. In this case, the threshold value is 94, as shown in Fig.4b. Finally, the Canny algorithm is used to extract the edges of the binary image and the resultant image is shown in Fig.4c.

2.2 Melt pool width extraction based on edge iterative model

2.2.1 Melt pool width extraction

During the deposition process, the melt pool formed by laser-melted powder is theoretically circular, which is determined by the light spot. However, the slow cooling rate at the end of melt pool often results in "trailing" phenomenon, leading to the elliptical melt pool, as shown in Fig.4c. This phenomenon changes the area and length of melt pool but does not affect the width of melt pool. The melt pool temperature indicates that the melting part of the powder has the highest temperature, resulting in the largest theoretical melt pool diameter. The theoretical circle always falls within the boundary regardless of the melt pool shape. Based on these analyses, the maximum inner tangent circle diameter (pixels) of the melt pool boundary is used as the melt pool width in this research.

Fig.5a shows the schematic diagram of the detection results of melt pool width. It can be seen that the melt pool width extracted by the maximum inner tangent circle algorithm is highly consistent with that obtained by manual measurement in Fig.4a. The calculation process is as follows.

(1) The pixel point in the melt pool image is set as $a_{i,j}$ with $i, j \in$[image width, image high].

(2) Define the set of contour points in Fig.4b as $Q[q_1, q_2, \cdots, q_n]$ with n as the number of profile points.

(3) Calculate the distances $g_{i,j}$ between the points in set Q and the point $a_{i,j}$, and then calculate the sum of all distances.

(4) Loop through Eq.(1) of all pixel points in the melt pool image, as follows:

$$g_{\max} = \begin{cases} g_{i,j}\,(g_{\max} < g_{i,j}) \\ g_{\max}\,(g_{\max} \geqslant g_{i,j}) \end{cases} \tag{1}$$

where $g_{\max}$ is the historical maximum distance and $g_{i,j}$ is the current iterative distance.

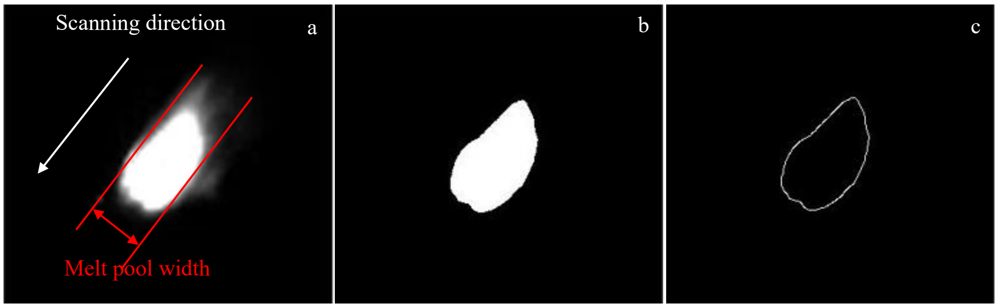

Fig.4 Pre-processing of melt pool image: (a) raw image; (b) binary image; (c) Canny edge extraction result

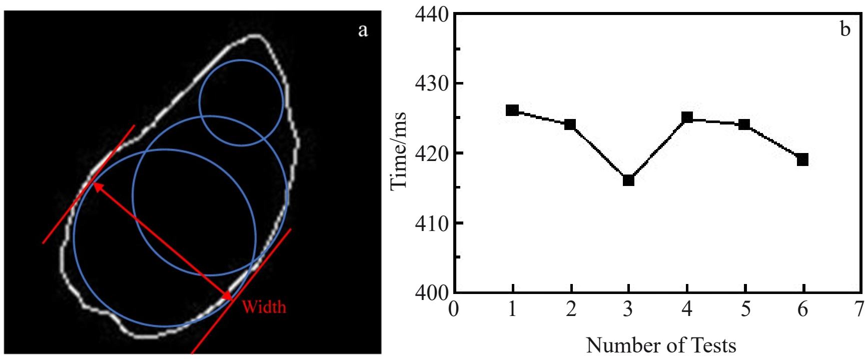

Fig.5 Melt pool width extraction process by algorithm method (a); calculation durations of algorithm in melt pool width extraction process (b)

(5) The coordinates of the pixel point corresponding to $g_{\max}$ are the center of the maximum inner tangent circle, and the diameter of the inner tangent circle is the width of melt pool.

Fig. 5b shows the calculation durations of the algorithm in the melt pool width extraction process. One image is treated six times to avoid systematic error, and the time consumption range of each cycle is controlled as 416−426 ms. It can be seen that the algorithm needs to iterate one iteration for each pixel point during the cycle. The numerous iterations result in time-consuming calculation, indicating that this algorithm is redundant.

2.2.2 Edge iterative model

The edge iterative model can be described as follows.

(1) As shown in Fig. 6a, the set of contour points Q is firstly counted. Three points (P_1, P_2, P_3) with point-to-point distances of one-third of the contour length are selected. The purpose of averaging sampling is to effectively avoid loops falling into the local optimum solution. Take one point as the intersection and connect it to other two points, as shown in Fig. 6b. P_2 is the intersection point, and the perpendicular bisector O_1M and O_1N of the P_2P_3 and P_2P_1 sides can be obtained, respectively. Draw the minimum enclosing circle around $\Delta P_1P_2P_3$ with the intersection point O_1 as the center and O_1P_3 as the radius. Therefore, the constrains are as follows:

$$\begin{cases} P_1,\ P_2,\ P_3 \in Q \\ MO_1 \perp P_2P_3,\ NO_1 \perp P_2P_1 \\ MP_2 = MP_3,\ NP_2 = N_1 \end{cases} \tag{2}$$

(2) If $\Delta P_1P_2P_3$ is not an acute triangle, the point should be re-selected until $\triangle P_1P_2P_3$ is an acute triangle.

$$\angle P_1, \angle P_2, \angle P_3 < 90° \tag{3}$$

(3) Find the edge point $P_{\min}$ in the circle with the smallest distance to point O_1 and replace the nearest point (P_1, P_2, or P_3) with $P_{\min}$ while still satisfying Eq.(2).

$$O_1P_{\min} \geqslant O_1P_1 \tag{4}$$

(4) Repeat the abovementioned step until there is no edge point $P_{\min}$ inside the circle O_i. At this time, the point O_i is the center of the circle inside the melt pool shape, and the distance O_iP_{i1} is the radius R of the circle.

As shown in Fig. 6b, the coordinates of point M, N, and O_i are (X_M, Y_M), (X_N, Y_N), and (X_O, Y_O), respectively. Then, the coordinates of the circle center can be represented by Eq. (5), as follows:

$$\begin{aligned} X_O &= \frac{(Y_M - Y_N)(Y_3 - Y_1)(Y_3 - Y_2) + X_M(X_3 - X_1)(Y_3 - Y_2) - X_N(X_3 - X_2)(Y_3 - Y_1)}{(X_3 - X_1)(Y_3 - Y_2) - (X_3 - X_2)(Y_3 - Y_1)} \\ Y_O &= \frac{(X_N - X_M)(X_3 - X_1)(X_3 - X_2) + Y_M(Y_3 - Y_1)(X_3 - X_2) - Y_N(Y_3 - Y_2)(X_3 - X_1)}{(X_3 - X_1)(Y_3 - Y_2) - (X_3 - X_2)(Y_3 - Y_1)} \end{aligned} \tag{5}$$

where (X_1, Y_1), (X_2, Y_2), and (X_3, Y_3) are the coordinates of point P_1, P_2, and P_3, respectively.

The radius of the circle can be calculated by Eq. (6), as follows:

$$R = \sqrt{(X_O - X_{i1})^2 + (Y_O - Y_{i1})^2} \tag{6}$$

The results of optimized algorithm extraction method are shown in Fig. 7. Fig. 7a and 7b show the first two iterations of the model, whereas Fig. 7c shows the final detection result. The iterative paths over the circle center during the algorithm calculation with five iterations are denoted by $O_1 - O_n$. The initial points of the iterative model are chosen randomly, leading to fluctuated algorithm detection durations. Fig. 7d shows the calculation durations of the optimized algorithm in the melt pool width extraction process. After model optimization, the average calculation duration sharply decreases from 422 ms to 3.75 ms.

2.3 Effectiveness of different methods for melt pool width detection

The algorithm calculation was conducted by Intel Core I5 1135 CPU with frequency of 2.40 GHz and 16 G RAM. The experiment parameters were as follows: powder feeding rate of 0.16 g/s, scanning speed of 10 mm/s, and laser power of 600 W. A circular deposition trajectory was selected for the printing scheme with an interlayer lift of 0.3 mm. Although machine learning methods are superior in the melt pool feature extraction in recent years[17–18], the large data quantity, high quality requirements of hardware, and poor real-time performance restrict their application only into the experiment stages. Therefore, in this research, the performance of the optimized algorithm was compared with that of traditional

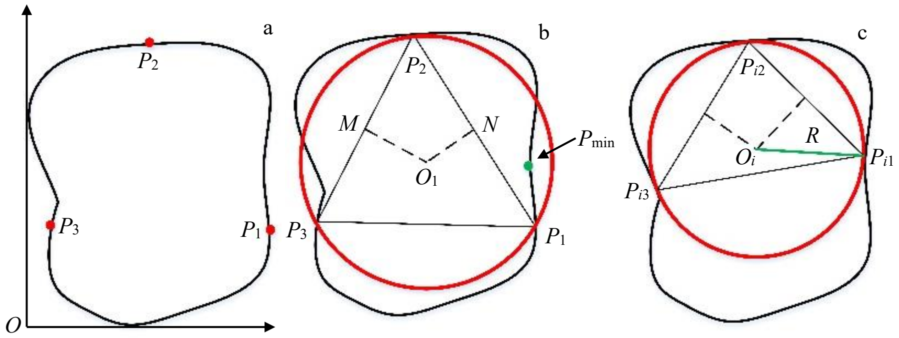

Fig.6 Schematic diagrams of edge iterative model of melt pool width extraction process: (a) set of contour points; (b) initial width extraction; (c) iterative width extraction

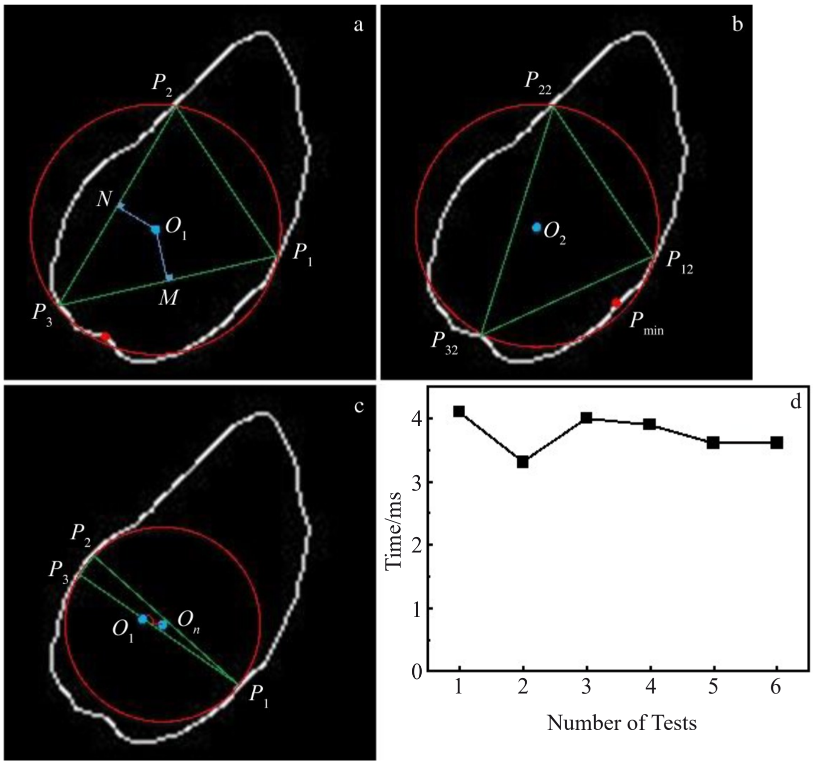

Fig.7 Melt pool width extraction process by optimized algorithm method: (a) the first iteration, (b) the second iteration, and (c) final iteration; calculation durations of optimized algorithm in melt pool width extraction process (d)

melt pool width extraction algorithms. The traditional focal distance (FD) method[9] and minimum bounding rectangle (MBR) method[13–14] were selected for comparison.

Fig.8 shows the schematic diagram with captured melt pool images and appearances of deposition sample and interference points. To validate the algorithm robustness, three levels (low, medium, and high) of interference melt pool images were selected for comparative analysis of melt pool width extraction. The spatial placement of these images was determined by the video timestamps. It should be noted that the actual location of the melt pool image may not coincide with the inferred spatial location due to the delay in image data transmission and machine movement, which causes the error of 1 ms. Nonetheless, the deposition layer corresponding to the melt pool image can still be identified, and the width of the same deposition layer remains relatively stable.

Hence, the microscopic-measured width of cross-section of the deposition layer is considered as the actual pixel width of the detected melt pool image. After measuring the melt pool width, the number of melt pool pixels was calculated from the pixel ratio, which was calibrated as 0.118 68 mm/pixel in this research. The algorithms predict the width by the number of image pixels.

Under each interference level condition, two groups of melt pool detection were conducted, and the L1, L2, M1, M2, H1, and H2 represent the detection groups under low, medium, and high interference level. For comparison, the raw images, FD algorithm results, MBR algorithm results, and optimized

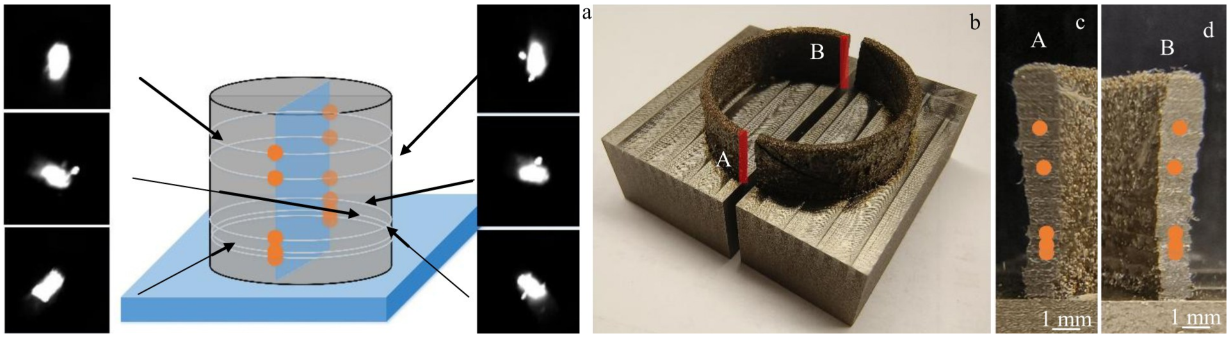

Fig.8 Schematic diagram with captured melt pool images (a) and appearances (b–d) of deposition sample and interference points: (b) overall appearance; (c) cross-section A; (d) cross-section B

algorithm results are shown in Fig. 9 – Fig. 11. FD algorithm uses the Canny algorithm to extract the melt pool edge, finds a straight line perpendicular to the scanning direction, and measures the maximum distance between the two intersections of the line and the melt pool edge as the melt pool width. MBR algorithm calculates the minimum outer rectangle of the melt pool edge. The length of the short side of the rectangle is considered as the melt pool width.

Table 2 presents the melt pool width results obtained by different algorithms. Fig. 12a shows the error of three algorithms. Although FD method has very high detection accuracy (the error is less than 1 pixel under low interference condition), its robustness is relatively low. Particularly, the calculation error occurs when the interference, such as spatter and arc light, is distributed along the vertical direction of the scanning speed. MBR algorithm shows high detection accuracy with the error of less than 3 pixels under low interference condition. However, this algorithm is susceptible to interference, such as powder spatter, which may consider the spattered part of the edge as the wrapping target. Besides, MBR algorithm cannot deal with the situation that the melt pool width changes from the short side to the long side and the correct rectangular output edge cannot be deduced from the melt pool change. The optimized algorithm shows good

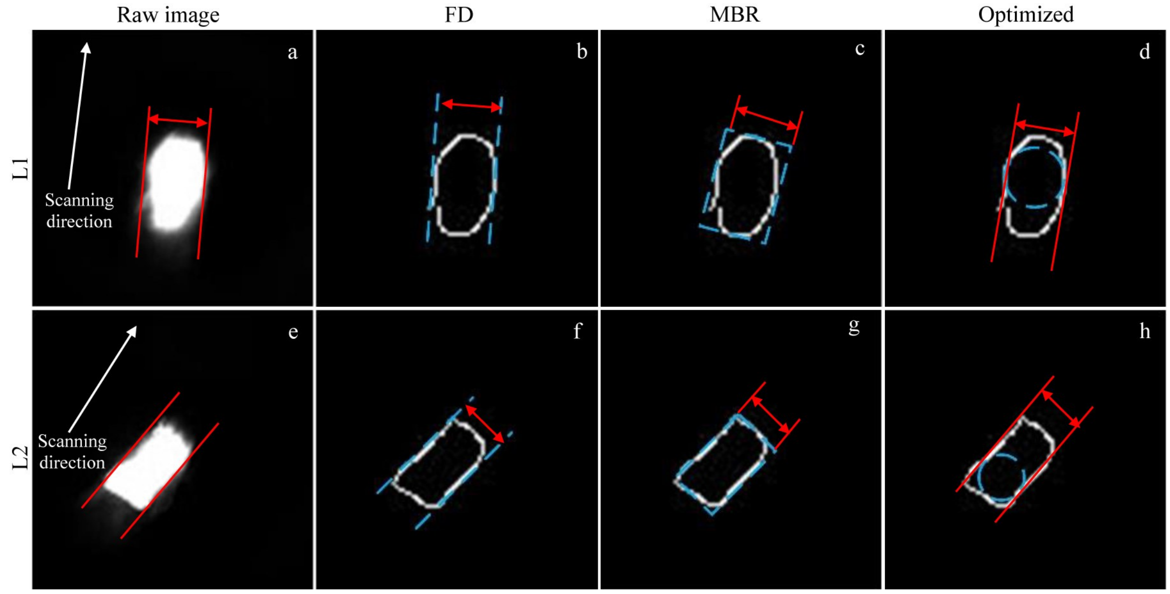

Fig.9 Melt pool image processing results under low interference condition: (a, e) raw images; (b, f) FD algorithm; (c, g) MBR algorithm; (d, h) optimized algorithm

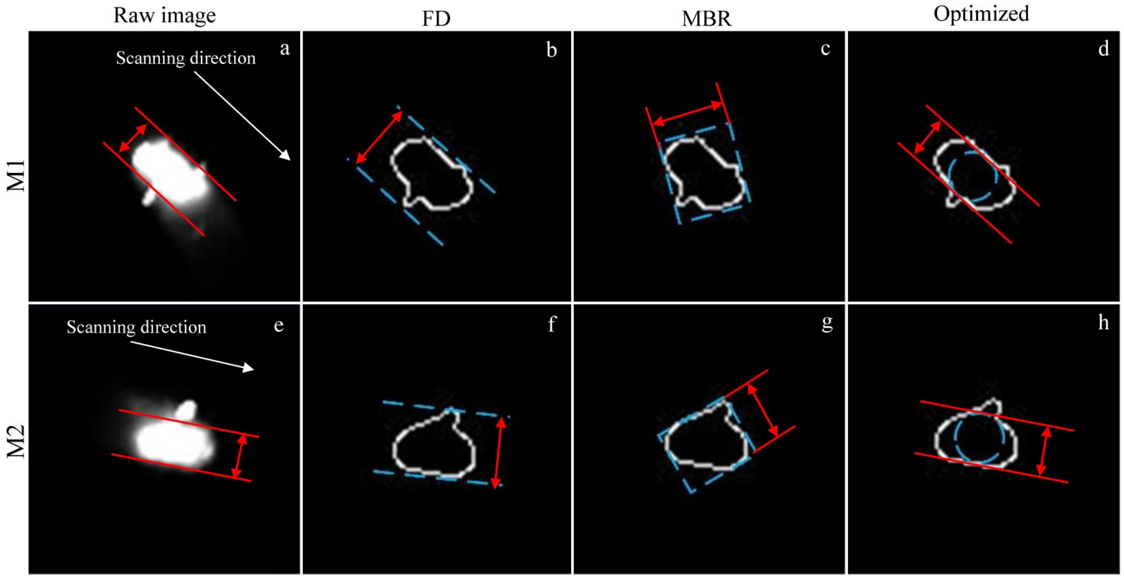

Fig.10 Melt pool image processing results under medium interference condition: (a, e) raw images; (b, f) FD algorithm; (c, g) MBR algorithm; (d, h) optimized algorithm

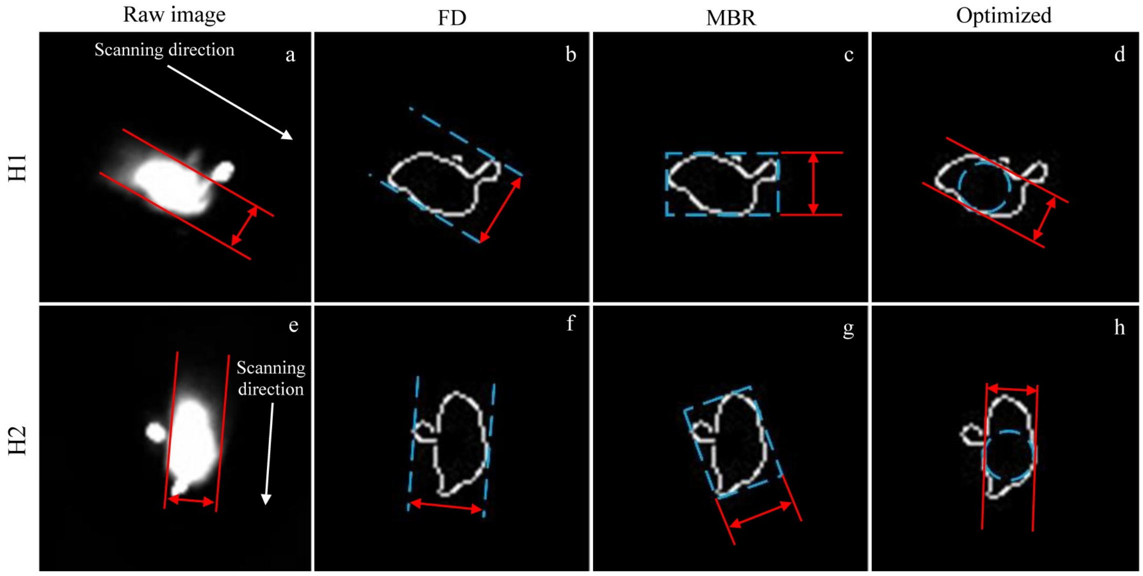

Fig.11 Melt pool image processing results under high interference condition: (a, e) raw images; (b, f) FD algorithm; (c, g) MBR algorithm; (d, h) optimized algorithm

Table 2 Melt pool width results obtained by different algorithms (pixel)

Interference level	Measurement	FD algorithm	MBR algorithm	Optimized algorithm
L1	16.3	16.5	17.9	16.6
L2	15.3	16.3	14.9	14.8
M1	15.7	21.3	21.5	14.9
M2	15.5	20.4	19.4	14.9
H1	15.6	22.3	17.5	15.4
H2	16.0	23.8	20.8	16.3

robustness against the interference, such as splash and arc light, and it ensures high detection accuracy with error of less than 1 pixel under different interference conditions.

Notably, the melt pool identification area is located at the rear of the scanning direction, as shown in Fig. 9f. This is because several significant interference may already gather in a short time at the rear position of the melt pool. This phenomenon causes error in the visualized algorithm calculation. The optimized algorithm determines the location of melt pool through the analysis of grayscale picture. The grayscale range is 0–255, but the grayscale value of the actual melt pool can exceed 255. However, the exceeding portion is still displayed as 255 in the image. The small spot size (<1.2 mm) may cause obvious powder splash and arc light. When multiple interference is concentrated in the rear area of melt pool, the reflected light intensity is close to 255 at some locations, showing brightness close to that of the melt pool. Thus, it is difficult to distinguish the splash from the actual melt pool. However, the probability of this phenomenon is relatively low. Different algorithms have their specific advantages, and they all should be further investigated.

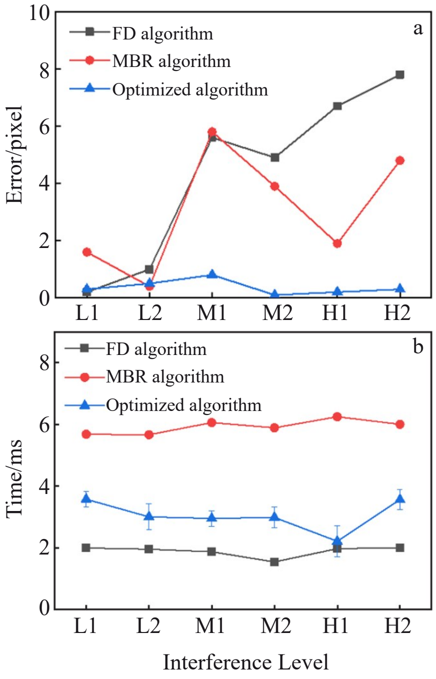

Fig.12 Error (a) and time consumption (b) of three algorithms for melt pool width detection

Fig.12b shows the time consumption of three algorithms for melt pool width detection. The average time consumption of the optimized algorithm is 2.55 ms, and all results are less than 4 ms. Due to the random selection of the initial points, the optimized algorithm has a more significant fluctuation in detection duration than other algorithms, and its maximum standard error is 0.5 ms. FD algorithm uses the least time with the average time consumption of 1.89 ms. The average time consumption of MBR algorithm is 5.92 ms. The standard error of these two algorithms is less than 0.03 ms, which can be ignored in this research. The purpose of online detection of

LDED melt pool width is to provide data for subsequent feature control. The delay of mainstream Modbus, RS-232, and serial communication is 10 – 20 ms, considering the feedback algorithm processing time and other hardware delays. Thus, the time consumption of a single cycle is usually longer than 25 ms. Clearly, the optimized algorithm meets the requirements.

Briefly, the optimized algorithm can accurately identify the width of melt pool under different working conditions and has good robustness against various types of noise.

2.4 Experiment and analysis

Deposition experiments were conducted to validate the feasibility and adaptability of the proposed approach. Single-track deposition was chosen as the experiment method. On the one hand, single-track deposition can avoid variable introduction, such as overlap ratio and interlayer lift, which can affect the accuracy of deposition width measurement. On the other hand, single-track deposition can reduce the deposition time and material consumption.

Based on the single-track deposition experiments, the process range was determined: laser power of 400 – 800 W, powder feeding rate of 0.25 – 0.35 g/s, and scanning speed of 9–11 mm/s. In this case, the formation quality can be ensured. An orthogonal experiment design was devised based on this parameter range: the interval of laser power was 200 W, the interval of scanning speed was 1 mm/s, and the interval of powder feeding rate was 0.05 g/s. The experiment parameters and results are shown in Table 3.

Fig. 13 shows the overall morphologies as well as melt pool images and metallographic results at point A (25 mm away from the beginning side) of different single-track deposition specimens corresponding to those in Table 2. The total track length is 50 mm. The melt pool widths at the beginning and end of the single-track deposition specimen show uneven phenomena, which is caused by the running mechanism that the acceleration and deceleration occur at both ends of the deposited track. Therefore, a buffer zone of 10 mm is left at both ends of the deposition track. The melt pool width was extracted by camera and the specimens with length of 30 mm in the middle of the layer were used for analysis. After the samples were cut, the mean values of the melt pool widths of the cross-sections with the distance of 10, 25, and 40 mm from the beginning side are taken as the actual widths of the melt pool.

Non-uniform powder accumulation can be observed in the cross-section along the deposition track. This phenomenon may be attributed to the non-vertical alignment between the processing head and the substrate, or the uneven powder distribution, which causes uneven powder aggregation at the laser focus and thereby affects the deposition morphology. However, this influence has a relatively minor effect on the melt pool width and can be ignored during measurement.

Fig. 14a shows the melt pool width comparison between measured results and algorithm calculation results. The experiment results show that the algorithms mentioned in this research are practical for melt pool width extraction within the specific processing parameters. The overall FD and MBR extraction results are high, and FD algorithm method has the highest average relative error of 12.67%, as shown in Fig. 14b. The melt pool width extracted by FD algorithm method is proportional to the interferences with direction perpendicular to the scanning direction. The average relative error of MBR algorithm method is 8.44%. MBR algorithm method adjusts the rectangular profile with the existence of interferences, thereby reducing the width extraction error to some extent. However, along the width detection, the extracted values are inaccurate.

Compared with FD and MBR algorithm methods, the detection algorithm of melt pool width based on the edge iterative model shows higher accuracy and better robustness, and its average relative error is only 2.46%. This is mainly due to the numerous interference in the melt pool area and the complicated boundary variation. At the same time, the optimized algorithm has high resistance against the boundary variation and can therefore detect the melt pool edge in more practical situations.

Fig. 14b illustrates the relative error of different algorithms for melt pool width detection. It can be seen that with increasing the laser power, the relative error of different algorithms is decreased. This can be attributed to the increased melt pool width, which results from higher laser power, thereby reducing the relative ratio between interference and melt pool. The algorithms mentioned in this research all maintain the high detection accuracy under different

Table 3 Experiment parameters and melt pool width results

Specimen No.	Laser power, P/W	Scanning speed, V/mm·min^{-1}	Powder feeding rate, G/g·s^{-1}	Melt pool width/mm
1	300	480	0.25	1.41
2	300	600	0.35	1.22
3	300	720	0.30	1.16
4	500	480	0.35	1.81
5	500	600	0.30	1.69
6	500	720	0.25	1.58
7	700	480	0.30	2.22
8	700	600	0.25	2.12
9	700	720	0.35	2.00

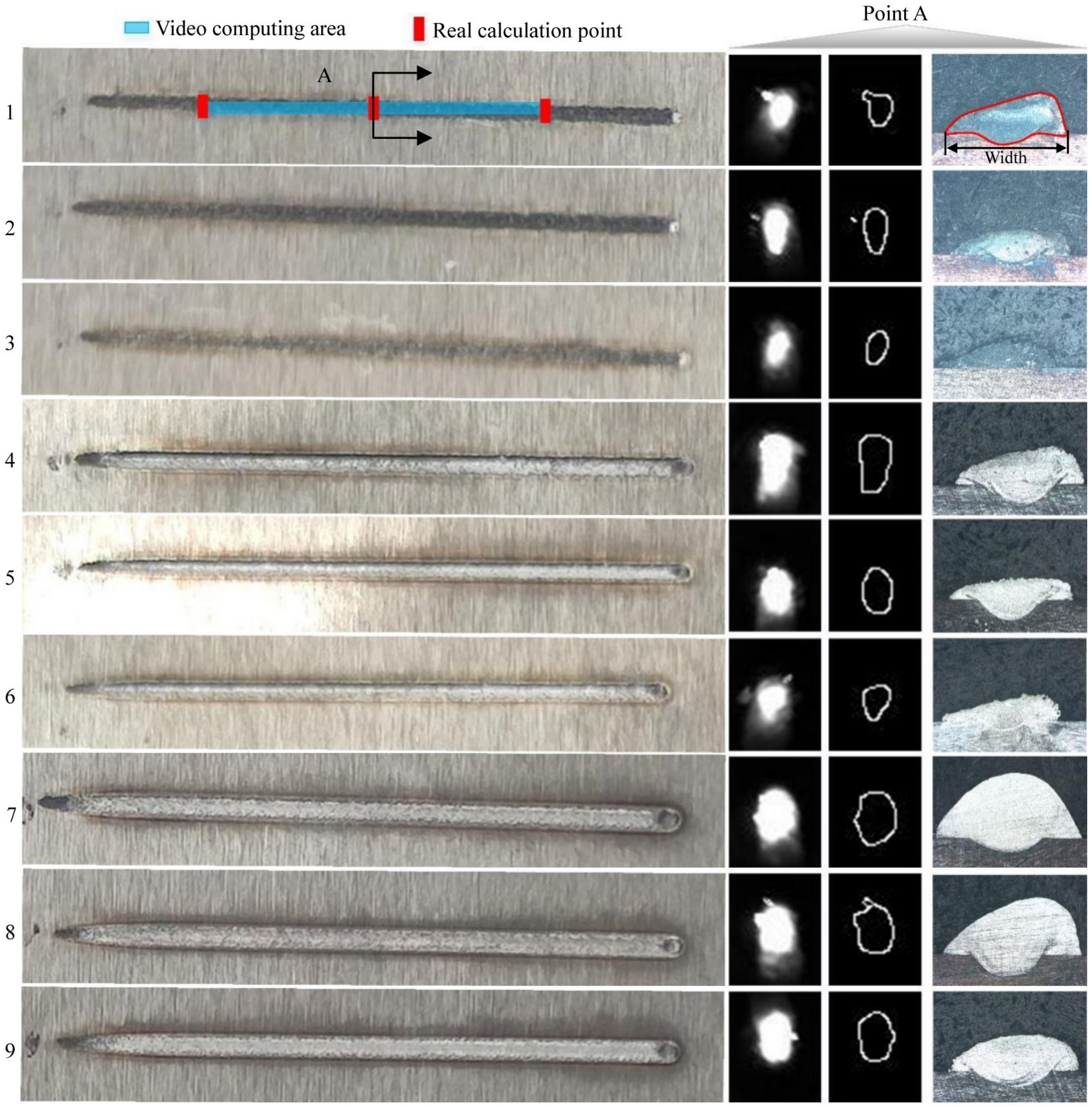

Fig.13 Overall morphologies as well as melt pool images and metallographic results at point A of different single-track deposition specimens

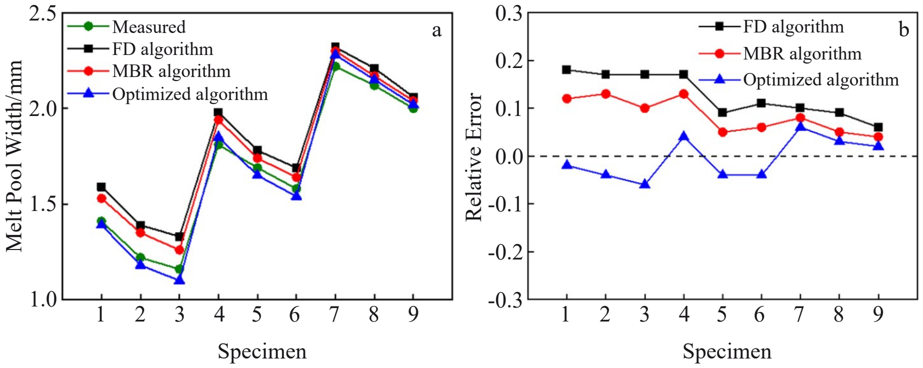

Fig.14 Melt pool width comparison between measured results and algorithm calculation results (a); relative error of different algorithms (b)

experiment parameters. Additionally, with increasing the laser power, the detected values obtained by optimized algorithm are firstly lower than the actual ones and then higher than the actual ones. It can also be observed that the melt pool images become brighter with increasing the laser power. It is inferred that the increased reflected light intensity under high power conditions causes overexposure of the camera. The exposure time should be reduced. The processing efficiency of optimized algorithm is worse than that of the traditional detection algorithms, but the optimized algorithm has excellent detection accuracy and high robustness. These advantages can be further improved by adaptive exposure to enhance the data acquisition accuracy and dynamic acquisition range. Briefly, the optimized algorithm method considers the laser energy distribution and the laws of powder metallurgy forming changes, which thereby exhibits excellent robustness and high extraction accuracy. The detection efficiency can meet the requirements of industrial online detection.

3 Conclusions

1) In LDED image recognition, interference, such as powder splash and arc light, may lead to inaccurate detection of melt pool width. The traditional algorithm for melt pool width extraction has restrictions due to the boundary features of the melt pool.

2) The optimized algorithm method considers the laser energy distribution and the laws of powder metallurgy forming changes, which thereby exhibits excellent robustness and high extraction accuracy. The detection efficiency can meet the requirements of industrial online detection.

3) The optimized algorithm can effectively extract the melt pool width under various process parameters, and the calculated results and measured results are in good agreement. The average error of the optimized algorithm is only 2.46%.

References

1 Qin L Y, Wang K, Li X D *et al. Chinese Journal of Mechanical Engineering: Additive Manufacturing Frontiers*[J], 2022, 1(4): 100052

2 Lin X, Zhu K, Fuh J Y H *et al. ISA Transactions*[J], 2022, 120: 147

3 McCann R, Obeidi M A, Hughes C *et al. Additive Manufacturing*[J], 2021, 45: 102058

4 Xue Sa, Wang Qingxiang, Liang Shujin *et al. Rare Metal Materials and Engineering*[J], 2023, 52(5): 1943 (in Chinese)

5 Qi X, Chen G, Li Y *et al. Engineering*[J], 2019, 5(4): 721

6 Tang Z, Liu W, Wang Y *et al. The International Journal of Advanced Manufacturing Technology*[J], 2020, 108: 3437

7 Tan C L, Li R S, Su J L *et al. International Journal of Machine Tools and Manufacture*[J], 2023, 189: 104032

8 Liu H, Sun R, Bai R *et al. Rare Metal Materials and Engineering*[J], 2023, 52(10): 3433

9 Su Y Y, Wang Z F, Xu X *et al. Journal of Manufacturing Processes*[J], 2022, 82: 708

10 Zheng L P, Zhang Q, Cao H Z *et al. Materials & Design*[J], 2019, 183: 108110

11 Sun Z, Wei G, Li L. *Optics & Laser Technology*[J], 2020, 129: 106280

12 Le T N, Lee M H, Lin Z H *et al. Journal of Manufacturing Processes*[J], 2021, 68: 1735

13 Huang J F, Xue L, Huang J Q *et al. Journal of Mechanical Engineering*[J], 2019, 55(17): 41

14 Yang Q, Yuan Z J, Zhi X L *et al. Optics & Laser Technology*[J], 2020, 123: 105925

15 Jeon I, Liu Y, Ryu K *et al. Additive Manufacturing*[J], 2021, 47: 102295

16 Goossens L R, Hooreweder B V. *Additive Manufacturing*[J], 2021, 40(5): 101923

17 Liu Y, Sohn H, Ma Z *et al. Computers in Industry*[J], 2023, 148: 103882

18 Zhu Q M, Liu Z L, Yan J H. *Comput Mech*[J], 2021, 67: 619

19 Zheng C, Wen J T, Diagne M. *Journal of Dynamic Systems Measurement and Control*[J], 2020, 142(6): 061001

20 Colodron P, Farina J, Rodriguez-Andina J *et al. IEEE International Symposium on Industrial Electronics*[C]. Gdnask: IEEE, 2011

21 Ding Y, Warton J, Kovacevic R. *Additive Manufacturing*[J], 2016, 10: 24

22 Huang Y, Khamesee M B, Toyserkani E. *Optics & Laser Technology*[J], 2019, 109: 584

23 Chen D J, Li G, Wang P *et al. Finite Elements in Analysis and Design*[J], 2023, 223: 103971

24 Liu M, Liu Z Q, Li B K *et al. Journal of Materials Research and Technology*[J], 2023, 26: 5626

25 Song Wei, Cheng Yanhai, Tantai Fanliang *et al. Applied Laser*[J], 2021, 41(1): 183 (in Chinese)

26 Shrivastava A, Chakraborty S S, Mukherjee S. *Optics & Laser Technology*[J], 2021, 144: 107404

27 Liu Jian, Xiang Chaoqian, Wang Fanghua *et al. Journal of Mechanical Engineering*[J], 2018, 54(5): 166 (in Chinese)

基于边缘迭代模型的激光沉积熔池宽度预测方法

苗立国[1]，邢　飞[1,2]，柴媛欣[1]，闫成鑫[1]，刘伟军[1]

(1. 沈阳工业大学 机械工程学院，辽宁 沈阳 110870)

(2. 南京中科煜宸激光技术有限公司，江苏 南京 210038)

摘　要：根据熔池尺寸特征空间分布规律，提出了一种基于边缘迭代模型的熔池宽度预测方法。为了获得精确的熔池宽度，采用数学形态学的方法对熔池图像进行去噪，并用手动阈值的方法对熔池图像进行粗分割。之后利用Canny算法提取出熔池边缘。最后，使用边缘迭代模型进行边缘迭代，得到精分割后的熔池宽度。对比实验结果表明，该算法具有良好的检测精度和鲁棒性，且简易高效。

关键词：激光金属沉积制造；熔池；边缘迭代模型；特征提取

作者简介：苗立国，男，1992年生，博士生，沈阳工业大学机械工程学院，辽宁 沈阳 110870，E-mail：miaoliguo@smail.sut.edu.cn